Combustion and Flame 221 (2020) 86–93

Contents lists available at ScienceDirect

Combustion and Flame

journal homepage: www.elsevier.com/locate/combustflame

On band lumping, radiation reabsorption, and high-pressure effects in laminar flame propagation

Shu Zheng[a,b], Ran Sui[b], Wenkai Liang[b,*], Huaichun Zhou[a], Chung K. Law[b]

[a] School of Energy, Power and Mechanical Engineering, North China Electric Power University, Beijing 102206, China
[b] Department of Mechanical and Aerospace Engineering, Princeton University, Princeton, NJ 08544, United States

ARTICLE INFO

Article history:
Received 13 March 2020
Revised 28 July 2020
Accepted 29 July 2020

Keywords:
Radiation reabsorption
Burning flux
Elevated pressures
SNBCK

ABSTRACT

Effects of radiation reabsorption on the burning flux of freely propagating laminar premixed flames at atmospheric and elevated pressures were numerically investigated for $CH_4/O_2/N_2/CO_2$ mixtures. Models with SNBCK 9 bands and 7 bands based on the spectral band lumping for H_2O, CO_2, CO and CH_4 were developed to improve the computational efficiency. It is found that the burning flux is promoted by the upstream radiation reabsorption and with increasing CO_2 concentration. Furthermore, with increasing pressure, radiation reabsorption first increases and then reduces the burning flux because of the corresponding increases of the reabsorption efficiency and the optical thickness, respectively. The blockage of radiation emission from the burnt mixture due to the increased optical thickness is dominant with the addition of the stronger radiative species CO_2 at higher pressures. Extensive computation further demonstrates that, compared with the benchmark case of 367 bands, the SNBCK 9 bands lumping retains good accuracy while substantially facilitates the computational efficiency.

1. Introduction

In addition to heat conduction, radiation is a major mode of heat transfer in combustion systems, with heat loss through emission and heat gain through reabsorption. These in turn would affect the flame temperature, the temperature-sensitive reaction rates, the extent of thermal conduction, and the global flame phenomena such as the flame propagation rate and the thresholds of extinction, flashback and blowoff [1,2]. Important as it is, systematic analytical and computational studies of radiation-affected phenomena have been challenged by the immensely complex species-dependent integro-differential equations governing its transport, leading to simplifying efforts at various levels of accuracy and the possible obscuring of certain controlling physics.

There are two objectives of the present study. First, we shall apply a band-lumping formulation, developed in heat transfer studies, to the problem of flame propagation, and demonstrate that there is an optimum number of bands, 9 in the present investigation, that is both physically accurate and computationally facilitating. Because of the generality of the formulation, the potential utility of the 9-band lumping formulation in the simulation of combustion phenomena is suggested. The second objective is to use this computationally efficient formulation to study the impact of radiation emission and reabsorption on the structure and propagation of the prototypical freely propagating planar premixed flame, especially in the practically important high-pressure environments, recognizing that the comprehensiveness and accuracy of previous worthwhile studies [2,3] have been challenged by the high demand of the computation cost.

To briefly substantiate the above statements, it is noted that in terms of the various useful radiation models that have been either adopted or developed in flame simulations, Buckmaster and Ronney [4] first used a gray gas model to study the radiation effect on the dynamics of flame balls, while Ju et al. [5] proposed improved Planck mean absorption coefficients for H_2O, CO_2 and CO to investigate the radiative heat loss on flame bifurcation in counterflow flames, and examined the accuracy of Tien's data [6]. Since the gas absorption coefficient used in optically thin models only considers the temperature dependence and ignores radiation reabsorption, Ju et al. [7] studied radiation reabsorption in the planar methane flame by considering the spectral dependence based on the statistical narrow-band (SNB) model, while Chen et al. [2] proposed a fitted statistical narrow-band correlated-*k* (FSNB-CK) model to calculate the radiative reabsorption in CH_4/air flames [8], as well as large-scale spherical flames [9] by solving the radiative transfer equation (RTE) using the discrete ordinate method (DOM) [10].

Recognizing the high computational cost for both SNB and FSNB-CK models, for example there are a total of 367 bands

* Corresponding author.
E-mail address: wenkail@princeton.edu (W. Liang).

https://doi.org/10.1016/j.combustflame.2020.07.042
0010-2180/

needed to be solved for the RTE when the bandwidth is 25 cm^{-1} for wave numbers from 150 cm^{-1} to 9300 cm^{-1}, Liu et al. [3] proposed a band lumping strategy to formulate a wideband CK model based on SNBCK. Thus instead of solving the RTE multiple times for each narrow band in the wideband, radiative transfer over the wideband is calculated by lumping several successive narrow bands into a single wideband. The reduction in the computation cost is however expected to be accompanied by reduced accuracy since the Plank blackbody function cannot be considered as constant with the wide bandwidth.

Considering the competing roles of computational accuracy and cost, we aim to assess the effects of spectral band numbers on these two computational parameters: clearly substantial loss in accuracy would not justify the reduction in the cost as the band number is reduced to a certain level. Here we note that Liu et al. [3] has demonstrated that an 18 band lumping incurred practically no loss in the radiation parameters. Consequently we aim to assess to what level of further reduction in the band number and the associated cost, as well as for multicomponent combustion systems, such accuracy can be largely maintained. We shall demonstrate in due course that the SNBCK 9 band lumping seems to exhibit an optimal range of accuracy-vs-cost.

Furthermore, in order to also gain further understanding on the role of radiation on laminar flame propagation, we shall extend the worthwhile work of Refs. [2,7] in assessing the influence of radiation reabsorption, especially in preheating the upstream region as it directly elevates the temperature of the reaction zone and hence Arrheniusly facilitates the reaction rates. The role of elevated pressure, which has not been adequately studied, is of particular interest because of its direct influence on the optical thickness, which increases with increasing pressure and hence reduces the extent of reabsorption, and as such counteracts the opposing effect due to the correspondingly increased absorptivity.

2. The SNBCK model and numerical method

For an isothermal and uniform medium with path-length L, mole fraction of the radiant gas X and pressure P, the narrow band averaged transmissivity in the SNB model can be expressed as [11]:

$$\bar{\tau}_\eta(L) = \exp\left[-\frac{\pi B}{2}\left(\sqrt{1+\frac{4SL}{\pi B}}-1\right)\right] \tag{1}$$

where, $B = 2\bar{\beta}_\eta/\pi^2$, $S = \bar{\kappa}_\eta XP$ and $\bar{\beta}_\eta = 2\pi\bar{\gamma}_\eta/\bar{\delta}_\eta$. The mean narrow-band parameters $\bar{\gamma}_\eta$, $\bar{\delta}_\eta$ and $\bar{\kappa}_\eta$ can be calculated according to Young's band model [12].

The line parameters used in this paper are based on the HITRAN 2016 database [13]. The temperature range is from 300 to 2900 K, and the corresponding spectral range is from 150 to 9300 cm^{-1}. The gas averaged transmissivity in Eq. (1) can be expressed as the absorption coefficient distribution function $f(k)$ in the SNBCK model based on the inverse Laplace transformation [14]:

$$f(k) = \frac{1}{2}k^{-3/2}(BS)^{1/2}\exp\left[\frac{\pi B}{4}\left(2-\frac{S}{k}-\frac{k}{S}\right)\right] \tag{2}$$

The cumulative distribution function $g(k)$ is introduced for the non-isothermal inhomogeneous media calculation and is defined as $g(k) = \int_0^k f(k')dk'$. Substituting it into Eq. (2) yields:

$$g(k) = \frac{1}{2}\left[1-\mathrm{erf}\left(\frac{a}{\sqrt{k}}-b\sqrt{k}\right)\right] + \frac{1}{2}\left[1-\mathrm{erf}\left(\frac{a}{\sqrt{k}}+b\sqrt{k}\right)\right]e^{\pi B} \tag{3}$$

where $a = \sqrt{\pi BS}/2$, $b = \sqrt{\pi B/S}/2$ and $erf(x)$ is the error function specified by $erf(x) = \frac{2}{\sqrt{\pi}}\int_0^x e^{-t^2}dt$.

Based on the band lumping strategy, the cumulative distribution function of a wide band formed from N narrow bands is obtained by averaging $g_i(k)$ for the N narrow bands. Inversion of $g(k)$ yields the gas absorption coefficients at the wideband, which can be performed efficiently by using a Newton–Raphson iteration method described by Lacis and Oinas [15] and Liu et al. [16].The g-values for the mixture are calculated by Ref. [17].

The benchmark results are obtained for the bandwidth of 25 cm^{-1}, which corresponds to 367 bands used in the spectral range from 150 to 9300 cm^{-1}. Since Liu et al. [3,18] have already validated the high accuracy for radiative heat transfer cases using a reduced number of bands, to 18 bands where the bandwidth is 500 cm^{-1}, we shall study herein the accuracy and efficiency of 9 bands with bandwidth 1000 cm^{-1} and 7 bands with bandwidth 1200 cm^{-1}.

The radiative transfer equation (RTE) [19] can be solved in the rectangular coordinate using the DOM method [20]. The T_4 [21] angular quadrature set with 128 directions in the entire 4π solid angle were used in the DOM.

Once the radiative intensity field is obtained, the net radiative flux can be calculated as

$$\dot{q}_r = \sum_{i=1}^{N-band}\sum_{j=1}^{N-gauss} w_j k_{i,j}\left(\sum_{m=1}^{M} I_{i,j,m} - 4\pi I_{bi,j}(T)\right)\Delta\eta \tag{4}$$

where N-$gauss$ is the Gauss points, and w_j the corresponding weight factor. The absorption coefficient $k_{i,j} = XPk$, where X is the mole fraction and P the pressure, and k can be obtained by inverting Eq. (3) at a given quadrature point g_j. The four-point Gauss–Lobatto quadrature was adopted in this work.

To validate the radiation model in this study, the radiative source from a one-dimensional layer bounded by a black emitting wall at 300 K and atmospheric pressure was investigated. The parallel-plane space was divided into 20 uniform volumes and the thickness of the medium was 0.1 m, 1 m and 5 m, respectively. The 1D parallel-plane layer was filled with H_2O, CO_2, CO and CH_4, respectively. The radiative power distributions calculated by the SNBCK 367 bands, 9 bands, 7 bands and HITEMP 2010 are shown in Fig. 1. The results for H_2O, shown in Fig. 1(a), are in addition compared with the FSNB-CK calculations in Ref. [2], which shows that the SNBCK 367 bands can well reproduce the FSNB-CK results. Consequently, results calculated by the SNBCK 367 bands are used as the benchmark for the flame cases. The results calculated by HITEMP 2010 [22] are used as the benchmark for the 1-D layer cases. As shown in Fig. 2(a), the averaged relative error of radiative power is 9.52% for H_2O, while that calculated by the SNBCK 7 bands is larger than that by the SNBCK 9 bands. In terms of the CPU time, the SNBCK 367 bands model (34.6 s) is about 10.9 times slower compared to the 9 bands model (3.12 s), while the 9 bands model only needs 13% more CPU time than the 7 bands model (2.76 s). Considering its higher computational accuracy (see the average relative errors in Fig. 2), the 9 bands model clearly outperforms the 7 bands model. Consequently, recognizing the relatively larger inaccuracy of the 7 band model, in the following we will not specifically discuss results based on it, although the quantitative results are still included in the figures. The coefficients for the SNBCK 9 bands model are provided as supplementary material.

3. Effects of radiation reabsorption

Planar flames of $CH_4/O_2/N_2/Ar/CO_2$ mixtures, with $O_2/(O_2+N_2+Ar+CO_2)$=21%, were calculated using the PREMIX code [23]. The reaction rates and transport properties were evaluated by the CHEMKIN and TRANSPORT packages, respectively. The detailed methane reaction mechanism GRI Mech 3.0 was employed [24]. To quantify the radiation effects, five radiation models, i.e.

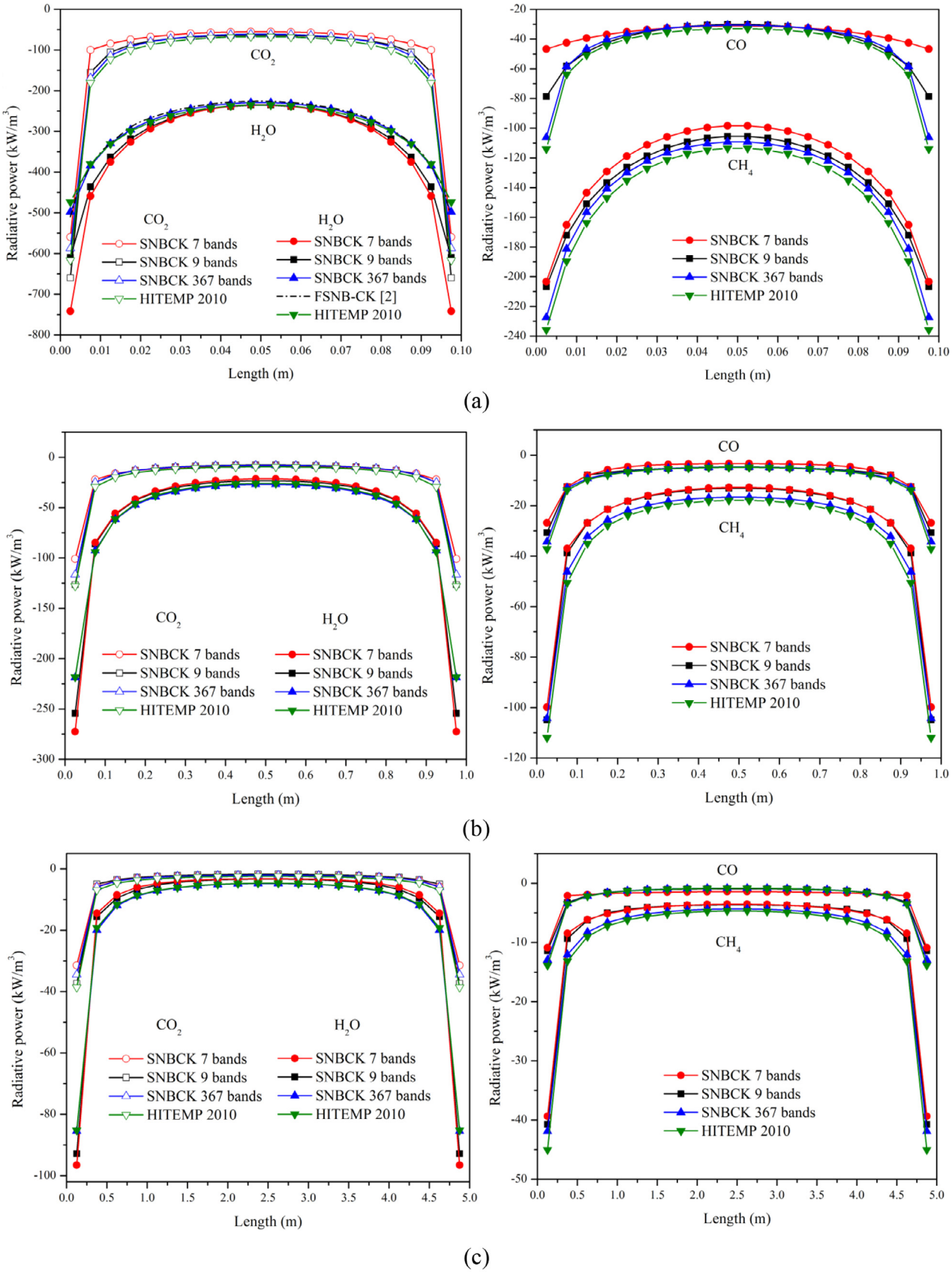

Fig. 1. Distributions of radiative power from a 1-D layer in a parallel-plane space at 1000 K, filled with H_2O, CO_2, CO and CH_4 for (a) $L = 0.1$ m, (b) $L = 1$ m and (c) $L = 5$ m.

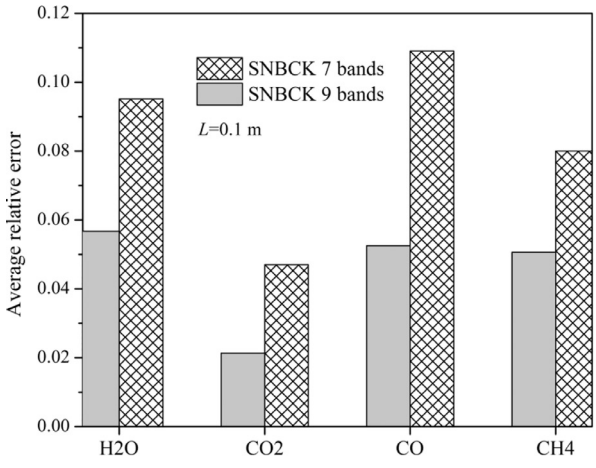

(a)

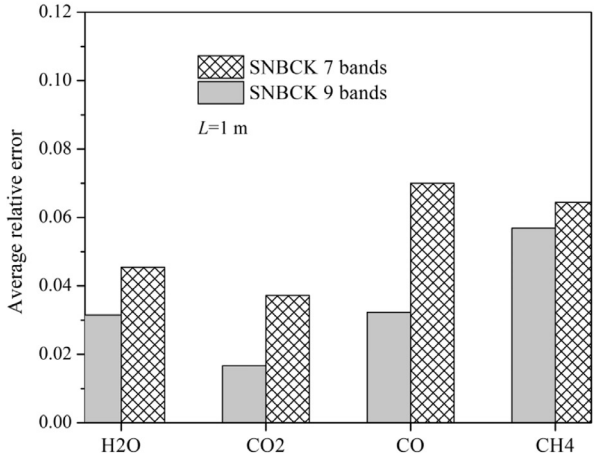

(b)

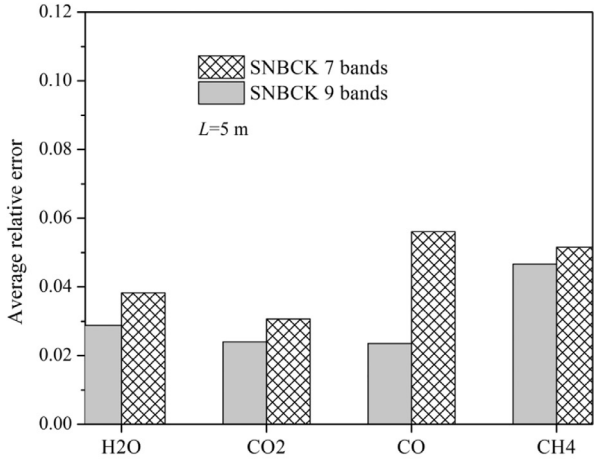

(c)

9

Fig. 2. Average relative error of radiative power for H_2O, CO_2, CO and CH_4 of the SNBCK 9 bands and 7 bands models at (a) $L = 0.1$ m, (b) $L = 1$ m and (c) $L = 5$ m.

ADI (adiabatic), OTM (optically thin model), SNBCK 367 bands, SNBCK 9 bands and SNBCK 7 bands, were applied in the simulations and compared. To assess the effects of different spectral band numbers on the radiation reabsorption, different amounts of CO_2, which is a strong absorber, were added in the unburned gas and partially substituted N_2. Furthermore, Ar dilution was used together with CO_2 dilution in the mixture to maintain the same mixture specific heat capacity. Consequently, the thermal effect of adding CO_2 is balanced with the Ar dilution and the pure effect of radiative heat loss is separated out.

The burning fluxes with different CO_2 percentages calculated by the five different radiation models for $CH_4/O_2/N_2/Ar/CO_2$ flames (ϕ=1.0) are shown in Fig. 3(a), demonstrating their different capabilities. First, the burning flux decreases with increasing CO_2 content due to the reduction of the flame temperature (from 2230 to 2150 K). Second, the burning fluxes of all the SNBCK models are higher than those of the ADI/OTM models. This is due to their inclusion of radiation reabsorption by the upstream unburned mixture as radiation reabsorption is only caused by CH_4 in the absence of CO_2. Third, the differences in the burning flux of the SNBCK 9 bands and the SNBCK 367 bands decrease progressively with increasing amount of CO_2. This is due to two reasons: first, the relative error of the radiative power calculated by the SNBCK 9 bands for CH_4 is larger than that for CO_2 (see Fig. 2); second, CO_2 has stronger absorption than CH_4 and hence the radiation reabsorption effect is dominated by the increased amount of CO_2 in the gas mixture. Specifically, with 3% CO_2, the relative increments of the burning flux calculated by the SNBCK 367 bands and 9 bands are 8.06% and 6.97%, respectively. However, when CO_2 addition is increased to 20%, the relative increments of the burning flux computed by the two SNBCK models are 18.6% and 18.3%, respectively. This indicates that the accuracy of the burning flux prediction becomes similar with increasing CO_2 percentage for the two models. As for the computational efficiency, the CPU times for solving RTE are: 1254.79 s for 367 bands and 109.88 s for 9 bands. Consequently, considering both the computational accuracy and efficiency, the SNBCK 9 bands model shows better performance than the 367 bands model. We have also calculated the burning fluxes by the full-spectrum correlated-k-distribution (FSCK) method [25] based on HITEMP 2010. As shown in Fig. 3(a), the FSCK-HITEMP predictions are in very good agreement with the SNBCK 367 bands predictions.

Figure 3(b) shows effects of different SNBCK models on the burning flux caused by the inclusion of radiation reabsorption of all species. Reabsorption can be assessed by comparing the system dimension to the Planck mean absorption length (Lp) of the burnt gas, defined as $Lp^{-1} = \int_0^\infty k(u)G(u)du$, and the optical thickness can be calculated by $\tau = L/Lp$ [7]. It is seen that the effect of radiation reabsorption becomes more important for $CH_4/O_2/N_2/Ar/CO_2$ mixtures with increased amount of CO_2, and is caused by the following two opposing trends. On one hand, this is due to the increased absorption coefficient with more CO_2, and thus more radiation reabsorption from upstream. On the other hand, the thermal radiation energy emitted by the products is blocked by the optical thickness τ of the burnt gas mixture, for which the maximum τ is only 0.053 in this case.

To understand the detailed structure of the radiation-affected flame, Fig. 4 shows how radiation reabsorption affects the burning flux, temperature and radiative heat loss distribution, calculated by ADI, OTM, SNBCK 367 bands, SNBCK 9 bands and SNBCK 7 bands, with 10% CO_2. With the reabsorption as demonstrated by using the SNBCK models, radiative heat loss is negative in the unburned region because radiation emitted from the high temperature downstream region is partially reabsorbed by the lower temperature gas. This leads to preheating the unburned mixture, such that the maximum temperature in the reaction zone ex-

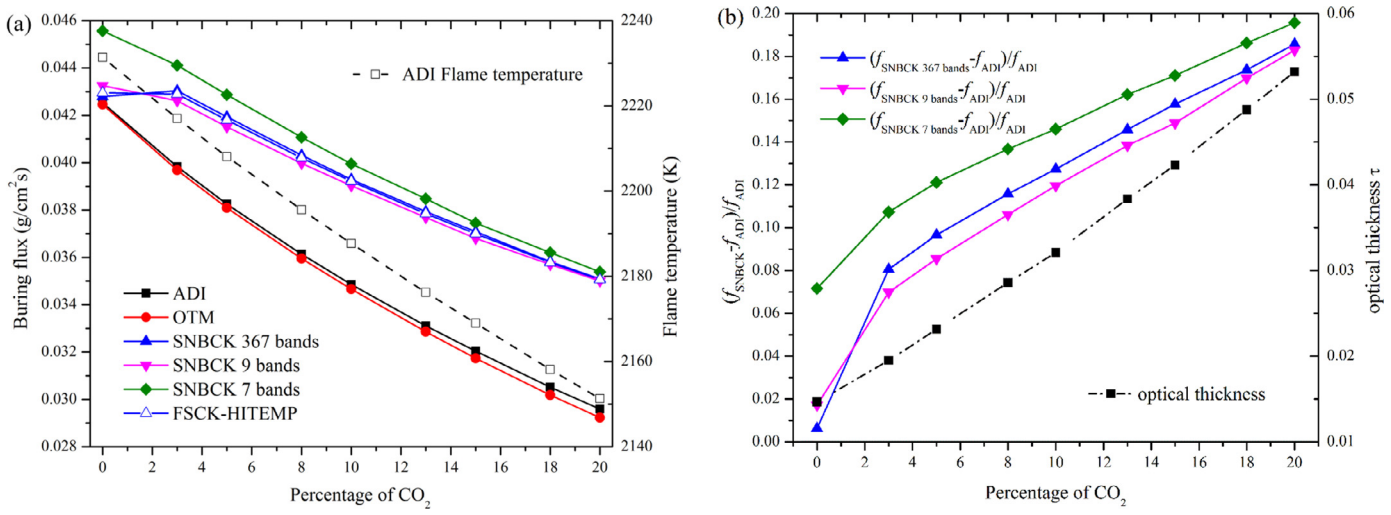

Fig. 3. (a) Burning flux as a function of CO_2 percentage calculated by different radiation models for a planar $CH_4/O_2/N_2/Ar/CO_2$ flames (ϕ=1.0); (b) Radiation reabsorption effects on the burning flux calculated by different SNBCK models and optical thickness as a function of CO_2 percentage.

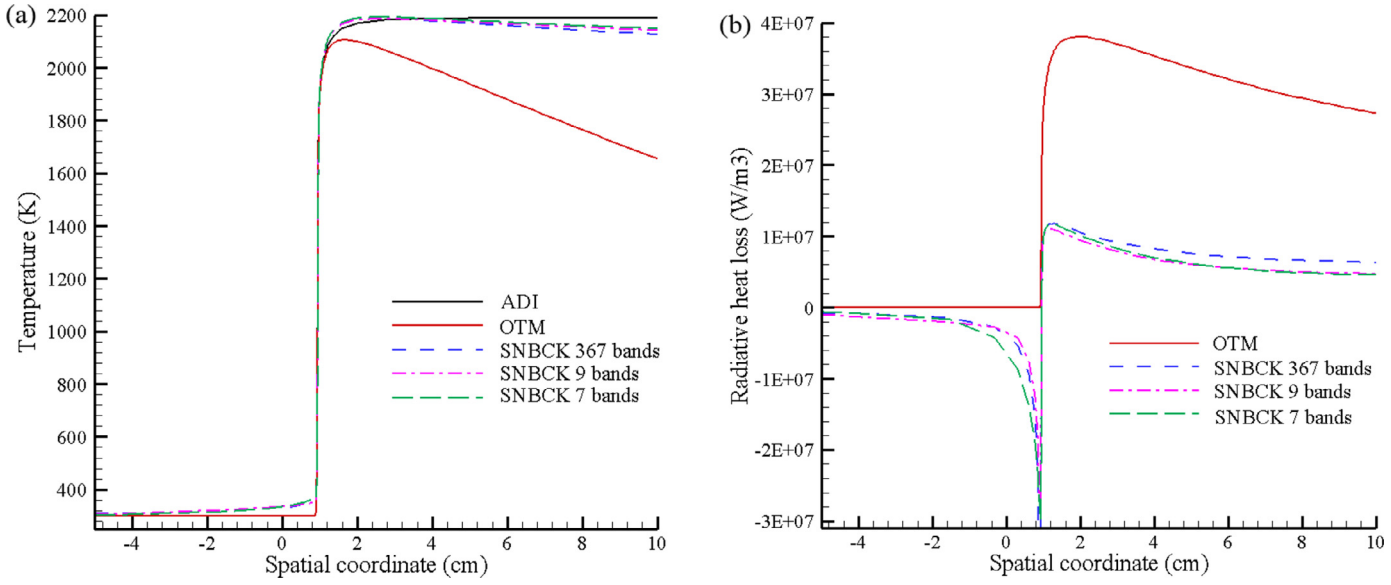

Fig. 4. Distributions of (a) temperature and (b) radiative heat loss in planar $CH_4/O_2/N_2/Ar/CO_2$ (ϕ=1.0, $CO_2/(O_2+N_2+Ar+CO_2)$=10%) flames.

ceeds the adiabatic flame temperature. This effect would further enhance the temperature-sensitive chain branching reactions such as H + O_2 = OH + O in the reaction zone. In addition, preheating in the diffusion zone would facilitate the chain initiation reactions such as the H-abstraction reaction for methane, which also has a high activation energy due to the strong C–H bond in methane. Such radiation emission-reabsorption effect provides an additional mechanism for heat re-distribution in the flame to heat conduction from the major downstream heat release CO + OH = CO_2 + H reaction.

4. Effects of pressure

We next examine the effects of pressure variation on the radiation reabsorption for the burning flux of CH_4/air flames. Fig. 5(a) shows the burning flux at pressures up to 25 atm calculated by different radiation models (ADI, OTM, SNBCK 367 bands, SNBCK 9 bands and SNBCK 7 bands) for CH_4/air flames (ϕ=1.0). Here we recognize that while the burning flux is expected to increase with pressure even without radiation heat transfer according to $f^0 \sim P^{n/2}$ [26], where n is the global reaction order, it could further increase due to upstream reabsorption and hence increase in the upstream temperature. Figure 5(b) shows the effects of different SNBCK models on the predicted burning flux and optical thickness as a function of pressure. It is found that the effects of radiation reabsorption first increase slowly with increasing pressure, but then decrease beyond 23 atm. This non-monotonic behavior is due to the fact that although the absorption coefficient of CH_4 increases with increasing pressure according to Eq. (4), the optical thickness however would increase from 0.016 to 0.35, which is six times larger than that in Fig. 3(b). At sufficiently high pressures, the optical thickness of the burnt mixture is so large that much of the thermal radiation energy is blocked and cannot reach the upstream unburned mixture. Consequently, the effect of radiation reabsorption is the result of the competition between these two effects.

The CPU times for solving RTE of CH_4/air (ϕ=1.0) flames are: 1655.26 s for SNBCK 367 bands and 156.34 s for SNBCK 9 bands. For P = 25 atm, the relative increments of f are 4.53% (367 bands) and 5.26% (9 bands). This indicates that as a compromise for the much lower computational cost (10 times faster than the SNBCK

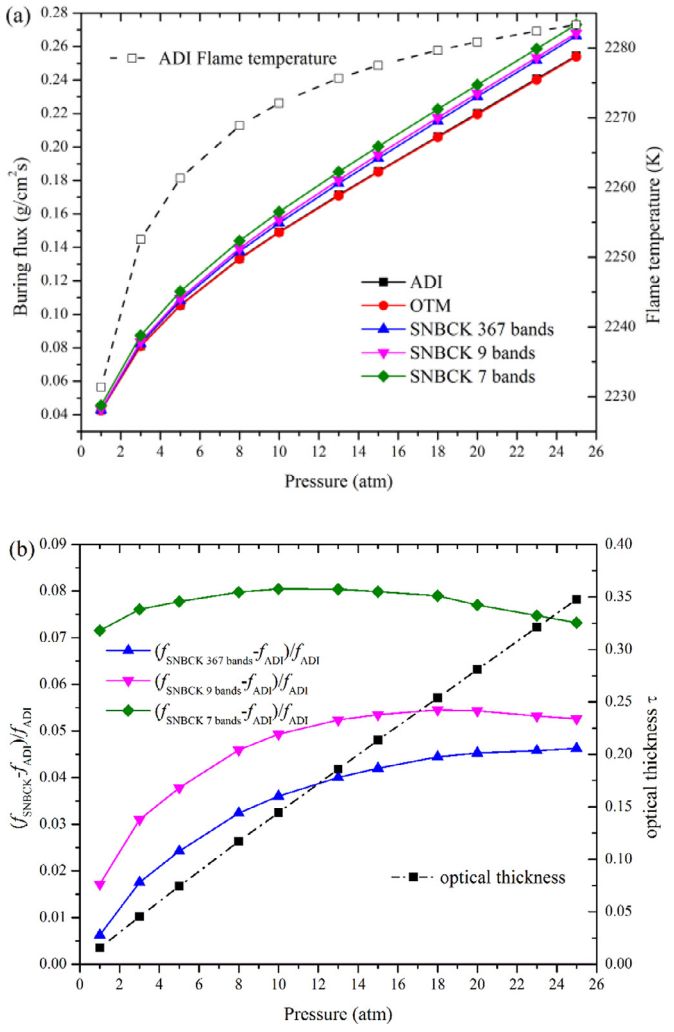

Fig. 5. (a) Burning flux of planar CH_4/air flames (ϕ=1.0) as a function of pressure calculated by the different radiation models; (b) Radiation reabsorption effects on the burning flux calculated by different SNBCK models and optical thickness as a function of pressure.

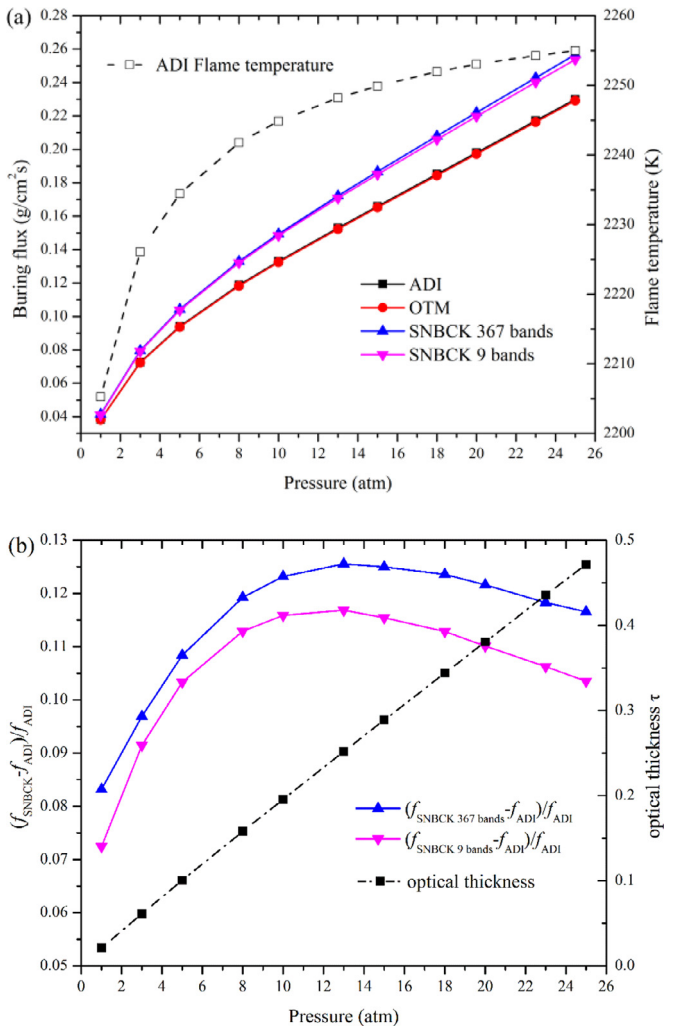

Fig. 6. (a) Burning flux $CH_4/O_2/N_2/CO_2$ flames (ϕ = 1.0, $CO_2/(O_2+N_2+CO_2)$ = 3%) as a function of pressure calculated by the different radiation models; (b) Radiation reabsorption effects on the burning flux calculated by different SNBCK models and optical thickness as a function of pressure.

367 bands), SNBCK 9 bands incurs a reduction in accuracy by only 16.1% as compared to SNBCK 367 bands. Consequently, the SNBCK 9 bands can be considered to be quite satisfactory in predicting the planar CH_4/air flames at elevated pressures.

In diesel engines, at excessive exhaust gas recirculation (EGR) conditions, radiation reabsorption of CO_2 reduces the radiation heat loss and even increases the flame speed through increasing the temperature of the unburned gas. To investigate this effect, we have added 3% CO_2 in the CH_4/air flames to mimic the EGR intake port in a modern diesel passenger car [27] to study the radiation reabsorption effects in planar $CH_4/O_2/N_2/CO_2$ flames at elevated pressures.

Figure 6(a) shows the burning fluxes at elevated pressures up to 25 atm calculated by using the different radiation models for $CH_4/O_2/N_2/CO_2$ flames (ϕ = 1.0, $CO_2/(O_2+N_2+CO_2)$=3%). Compared to the CH_4/air flames, the increase of the burning fluxes in the $CH_4/O_2/N_2/CO_2$ flames are more obvious when considering radiation reabsorption since the radiative property of CO_2 is stronger than that of CH_4. Figure 6(b) shows that the maximum radiation reabsorption effect calculated by the SNBCK 367 bands is 12.6% for the $CH_4/O_2/N_2/CO_2$ flame while it is only 4.63% for the corresponding CH_4/air flame. Moreover, the effect of radiation reabsorption decreases at pressures above 13 atm, which is earlier than that in the CH_4/air flame. The maximum τ is 0.47 larger than that of the CH_4/air flames. These results therefore demonstrate that the optical thickness becomes thicker with the addition of the stronger radiative species CO_2, hence leading to stronger blockage for radiation emission from the burnt gas.

The predicted average radiation reabsorption effects are 11.47% and 10.85% for the SNBCK 367 and 9 bands, respectively, with their corresponding CPU times of solving RTE being 1303.38 s and 120.81 s. This again demonstrates that the SNBCK 9 bands model not only maintains adequate accuracy but is also more computational efficient.

To illustrate how radiation reabsorption affects temperature at different pressures, Fig. 7 shows the temperature distributions calculated by SNBCK 367 bands for the $CH_4/O_2/N_2/CO_2$ flames at P = 1, 13 and 25 atm. It is seen that the flame temperature increases with increasing pressure and temperature in the upstream due to radiation reabsorption. However, the increment of temperature in the upstream at P = 13 atm is larger than that at P = 1 and 25 atm, as shown in the enlarged inset in Fig. 7. This is why the maximum radiation reabsorption effect on the burning flux occurs at P = 13 atm for the $CH_4/O_2/N_2/CO_2$ flames.

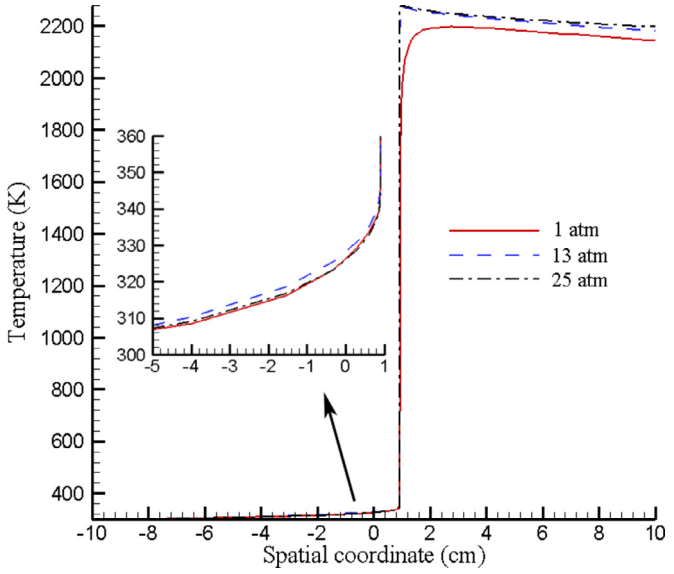

Fig. 7. Distributions of temperature calculated by the SNBCK 367 bands for planar $CH_4/O_2/N_2/CO_2$ flames (ϕ = 1.0, $CO_2/(O_2+N_2+CO_2)$=3%) at P = 1, 13 and 25 atm.

5. Conclusions

Effects of radiation reabsorption on the burning flux of methane flames at elevated pressures are investigated using SNBCK models. To facilitate the computational efficiency, an SNBCK 9 bands model for H_2O, CO_2, CO and CH_4 is employed and validated for the computation of planar flames with radiation.

Results demonstrate that radiation reabsorption increases the burning flux, which is further increased with CO_2 addition. As such, radiation reabsorption should be included in the quantitative analyses of flame structure and temperature, burning intensity and propagation rate, and other associated reaction and flame propagation quantities. Due to the competition between the absorption coefficient and optical thickness, the radiation reabsorption effect first increases and then decreases with increasing pressure. The addition of stronger radiative species such as CO_2 enhances blockage of the burnt mixture radiation emission effect at higher pressures. The 9 bands lumping appears to be an optimum number in terms of accuracy and computation cost, at least for the present problem studied. The potential of extending the concept of lumping, from the present procedure based on uniform lumping to one that depends on the structure of the radiation spectrum, merits further study.

Comparing results of the OTM without those allowing for reabsorption, Fig. 4 shows substantial downstream temperature reduction and hence heat loss without reabsorption. While effects of upstream reabsorption has been found to dominate over those of downstream reabsorption in the present study, there are two situations for which downstream heat loss and reabsorption are expected to be important and require further study. The first is for near-limit situations of radiation-induced extinction and flammability limit, for which simplified analysis [28] has shown that effects of upstream and downstream heat loss have equal influence on the extinction boundary; the latter through the increase in the (negative) temperature gradient in the downstream region next to the reaction zone and consequently the temperature in the reaction zone. The second is the effect of the temperature and hence density change in the downstream region due to the combined effects of radiation emission and reabsorption. This effect has been shown to substantially reduce the flame propagation rate for spherical flame propagation with closed flame surface [1], although the separate effects due to emission and reabsorption needs to be clearly identified.

Declaration of Competing Interest

The authors declare that they have no known competing financial interests or personal relationships that could have appeared to influence the work reported in this paper.

Acknowledgements

The research at Princeton University was supported in part by the US Air Force Office of Scientific Research. SZ participated in this research as a visiting research scholar at Princeton University, being supported by his home institution.

Supplementary materials

Supplementary material associated with this article can be found, in the online version, at doi:10.1016/j.combustflame.2020.07.042.

References

[1] Z. Chen, Effects of radiation and compression on propagating spherical flames of methane/air mixtures near the lean flammability limit, Combust. Flame 157 (2010) 2267–2276.
[2] Z. Chen, X. Qin, B. Xu, Y. Ju, F. Liu, Studies of radiation absorption on flame speed and flammability limit of CO2 diluted methane flames at elevated pressures, Proc. Combust. Inst. 31 (2007) 2693–2700.
[3] F. Liu, G.J. Smallwood, m.L. Oslash, Ider G-uacute, Band lumping strategy for radiation heat transfer calculations using a narrowband model, J. Thermophys. Heat Transf. 14 (2000) 278–281.
[4] D. Lozinski, J. Buckmaster, P. Ronney, Absolute flammability limits and flame-balls, Combust. Flame 97 (1994) 301–316.
[5] Y. Ju, H. Guo, F. Liu, K. Maruta, Effects of the Lewis number and radiative heat loss on the bifurcation and extinction of CH 4/O 2-N 2-He flames, J. Fluid Mech. 379 (1999) 165–190.
[6] C.-L. Tien, Thermal Radiation Properties of gases, in: Advances in Heat Transfer, Elsevier (1969), pp. 253–324.
[7] Y. Ju, G. Masuya, P.D. Ronney, Symposium (international) On Combustion, Elsevier (1998), pp. 2619–2626.
[8] C.H. Sohn, Z. Chen, Y. Ju, Effects of radiation on the uncertainty of flame speed determination using spherically propagating flames with CO/CO 2/H 2 O dilutions at elevated pressures, Int. J. Heat Mass Transf. 86 (2015) 820–825.
[9] Z. Chen, Effects of radiation on large-scale spherical flame propagation, Combust. Flame 183 (2017) 66–74.
[10] W. Fiveland, Discrete-ordinates solutions of the radiative transport equation for rectangular enclosures, J. Heat Transfer 106 (1984) 699–706.
[11] C.B. Ludwig, W. Malkmus, J.E. Reardon, J.A.L. Thomson, R. Goulard, Handbook of Infrared Radiation From Combustion Gases. Nasa sp-3080, NASA Special Publication (1973), p. 3080.
[12] S.J. Young, Nonisothermal band model theory, J. Quant. Spectrosc. Radiat. Transfer 18 (1977) 1–28.
[13] I.E. Gordon, L.S. Rothman, C. Hill, R.V. Kochanov, Y. Tan, P.F. Bernath, M. Birk, V. Boudon, A. Campargue, K. Chance, The HITRAN2016 molecular spectroscopic database, J. Quant. Spectrosc. Radiat. Transfer 203 (2017) 3–69.
[14] G. Domoto, Frequency integration for radiative transfer problems involving homogeneous non-gray gases: the inverse transmission function, J. Quant. Spectrosc. Radiat. Transfer 14 (1974) 935–942.
[15] A.A. Lacis, V. Oinas, A description of the correlated k distribution method for modeling nongray gaseous absorption, thermal emission, and multiple scattering in vertically inhomogeneous atmospheres, J. Geophys. Res. 96 (1991) 9027–9063.
[16] F. Liu, G.J. Smallwood, Ö.L. Gülder, Application of the statistical narrow-band correlated-k method to low-resolution spectral intensity and radiative heat transfer calculations — Effects of the quadrature scheme, Int. J. Heat Mass Transf. 43 (2000) 3119–3135.
[17] M.F. Modest, R.J. Riazzi, Assembly of full-spectrum k-distributions from a narrow-band database; effects of mixing gases, gases and nongray absorbing particles, and mixtures with nongray scatterers in nongray enclosures, J. Quant. Spectrosc. Radiat. Transfer 90 (2005) 169–189.
[18] F. Liu, G. Smallwood, O. Gulder, An accurate efficient and flexible SNBCK-based unified band model for calculations of spectrally resolved and integrated quantities in participating media containing real gases, Proceedings of the 12th International Heat Transfer Conference (2002), pp. 663–668.

[19] M.F. Modest, Radiative Heat Transfer, Academic Press, 2013.
[20] F. Liu, H. Becker, A. Pollard, Spatial differencing schemes of the discrete-ordinates method, Numer. Heat Transfer 30 (1996) 23–43.
[21] C. Thurgood, A. Pollard, H. Becker, The TN quadrature set for the discrete ordinates method, J. Heat Transfer 117 (1995) 1068–1070.
[22] P. Rivière, A. Soufiani, Updated band model parameters for H2O, CO2, CH4 and CO radiation at high temperature, Int .J Heat Mass Transf. 55 (2012) 3349–3358.
[23] R.J. Kee, J.F. Grcar, M.D. Smooke, J.A. Miller, E. Meeks, Sandia National Laboratories Report, 1985.
[24] Available at http://www.me.berkeley.edu/gri_mech/.
[25] C. Wang, W. Ge, M.F. Modest, B. He, A full-spectrum k-distribution look-up table for radiative transfer in nonhomogeneous gaseous media, J. Quant. Spectrosc. Radiat. Transfer 168 (2016) 46–56.
[26] F. Egolfopoulos, C.K. Law, Chain mechanisms in the overall reaction orders in laminar flame propagation, Combust. Flame 80 (1990) 7–16.
[27] M. Peckham, B. Campbell, A. Finch, Measurement of the effects of the exhaust gas recirculation delay on the nitrogen oxide emissions within a turbocharged passenger car diesel engine, proceedings of the institution of mechanical engineers, Part D: J. Automobile Eng. 225 (2011) 1156–1166.
[28] C.K. Law, Combustion Physics, Cambridge University Press, 2010.